Nonlinear traveling waves in a multilayer system

Ilya B. Simanovskii
Department of Mathematics, Technion–Israel Institute of Technology, 32000 Haifa, Israel
(Received 15 January 2009; published 26 May 2009)

The nonlinear convective regimes in multilayer system air-ethylene glycol-fluorinert FC75 heated from below under the joint action of buoyant and thermocapillary mechanisms of instability are investigated. The periodic boundary conditions on the lateral boundaries are considered. It is found that the competition of both mechanisms of instability may lead to the development of specific types of flow: buoyant-thermocapillary traveling wave and pulsating traveling wave.

DOI: 10.1103/PhysRevE.79.056313 PACS number(s): 47.20.−k, 47.35.Pq, 47.55.dm

I. INTRODUCTION

Convective phenomena in fluid systems with an interface have been a subject of an extensive investigation. There are two basic physical phenomena that produce convective instability in systems with an interface: buoyancy and thermocapillary effect. When heating is from below, the buoyancy instability generates the Rayleigh-Bénard convection [1], while the thermocapillary effect is the origin of the Marangoni-Bénard convection [2,3]. Buoyancy (a volume effect) is more important for relatively thick layers, while the thermocapillarity (an interfacial effect) plays the dominant role in the case of thin layers or under microgravity conditions. The case where buoyancy and thermocapillary effect act simultaneously is the most typical.

The joint action of both mechanisms of instability in a system with a single interface has been a subject of many investigations (for a review, see [3–5]). Specifically, the joint action of buoyancy and thermocapillary effect was studied for the convection in fluid layers heated from below [6,7], in fluid layers with horizontal temperature gradients [8–11], in the case of liquid bridges [12–14], for the flow around bubbles [15], etc.

The interfacial convection in *multilayer systems* is a widespread phenomenon that is of great importance in numerous branches of technology. Among the modern techniques requiring an investigation of convection in systems with many interfaces are liquid encapsulation crystal-growth technique [16,17] used in space laboratories missions, droplet-droplet coalescence processes, where Marangoni convection in the interdroplet film can considerably affect the coalescence time during extraction [18], and others. The three-layer systems can differ considerably from the systems with a single interface. The essentially new effect is the possibility of the interaction of the interfaces. In three-layer systems, it is possible to consider the "direct" interaction of thermocapillary and buoyancy mechanisms of instability (when both mechanisms act on one and the same interface) and the "indirect" interaction (when both mechanisms act on different interfaces). Simultaneous interaction of interfaces with their bulk phases and with each other was studied for heating from below and from above [19], [20,21], as well as in the case of horizontal temperature gradients [22–25].

The joint action of buoyancy and thermocapillary effect can lead to the appearance of the oscillatory instability when heating is from below. This phenomenon was first discovered in the case of a two-layer system [3,7,26]. A similar phenomenon under the joint action of both mechanisms of instability in the multilayer system with free or rigid heat-insulated lateral boundaries has been studied in [27]. Only regimes of standing waves have been obtained in [27].

In the present paper, we investigate the joint action of buoyant and thermocapillary mechanisms of instability in multilayer system air-ethylene glycol-fluorinert FC75 with *periodic boundary conditions* on lateral boundaries. It is found that the competition of both mechanisms of instability may lead to the development of different types of convective flows: nonlinear buoyant-thermocapillary traveling wave and pulsating traveling wave. These flows have not been found before.

The paper is organized as follows. In Sec. II, the mathematical formulation of the problem in a three-layer system is presented. The nonlinear approach is described in Sec. III. Nonlinear simulations of the finite-amplitude convective regimes are considered in Sec. IV. Section V contains some concluding remarks.

II. GENERAL EQUATIONS AND BOUNDARY CONDITIONS

Let the space between two rigid horizontal plates be filled by three immiscible viscous fluids with different physical properties (see Fig. 1). The equilibrium thicknesses of the layers are a_m, $m=1,2,3$. The mth fluid has density ρ_m, kinematic viscosity ν_m, dynamic viscosity $\eta_m=\rho_m\nu_m$, thermal diffusivity χ_m, heat conductivity κ_m, and heat expansion coefficient β_m. The surface-tension coefficients on the upper and lower interfaces σ and σ_* are linear functions of temperature T: $\sigma=\sigma_0-\alpha T$, $\sigma_*=\sigma_{*0}-\alpha_* T$. The acceleration due to gravity is g. The horizontal plates are kept at different constant temperatures. The system is heated from below, and the overall temperature drop is θ.

We define

$$\rho=\frac{\rho_1}{\rho_2},\quad \nu=\frac{\nu_1}{\nu_2},\quad \eta=\frac{\eta_1}{\eta_2}=\rho\nu,\quad \chi=\frac{\chi_1}{\chi_2},$$

$$\kappa=\frac{\kappa_1}{\kappa_2},\quad \beta=\frac{\beta_1}{\beta_2},\quad a=\frac{a_2}{a_1},$$

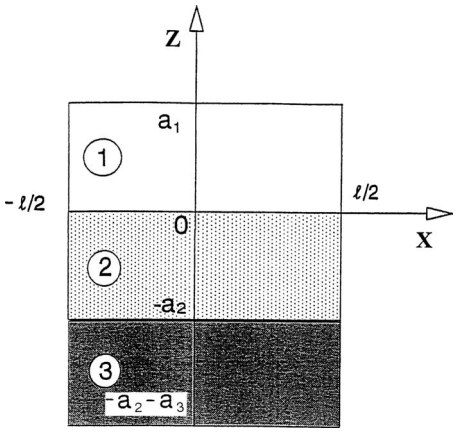

FIG. 1. Geometrical configuration of the three-layer system and coordinate axes.

$$\rho_* = \frac{\rho_1}{\rho_3}, \quad \nu_* = \frac{\nu_1}{\nu_3}, \quad \eta_* = \frac{\eta_1}{\eta_3} = \rho_* \nu_*, \quad \chi_* = \frac{\chi_1}{\chi_3},$$

$$\kappa_* = \frac{\kappa_1}{\kappa_3}, \quad \beta_* = \frac{\beta_1}{\beta_3}, \quad a_* = \frac{a_3}{a_1}, \quad \bar{\alpha} = \frac{\alpha_*}{\alpha}.$$

As the units of length, time, velocity, pressure, and temperature, we use a_1, a_1^2/ν_1, ν_1/a_1, $\rho_1\nu_1^2/a_1^2$, and θ. The complete nonlinear equations governing convection are then written in the following dimensionless form:

$$\frac{\partial \mathbf{v}_m}{\partial t} + (\mathbf{v}_m \cdot \nabla)\mathbf{v}_m = -e_m \nabla p_m + c_m \Delta \mathbf{v}_m + b_m G T_m \mathbf{e}, \quad (1)$$

$$\frac{\partial T_m}{\partial t} + \mathbf{v}_m \cdot \nabla T_m = \frac{d_m}{P} \Delta T_m, \quad (2)$$

$$\nabla \mathbf{v}_m = 0, \quad m = 1,2,3, \quad (3)$$

where $e_1=c_1=b_1=d_1=1$, $e_2=\rho$, $c_2=1/\nu$, $b_2=1/\beta$, $d_2=1/\chi$, $e_3=\rho_*$, $c_3=1/\nu_*$, $b_3=1/\beta_*$, and $d_3=1/\chi_*$; $\Delta=\nabla^2$, $G=g\beta_1\theta a_1^3/\nu_1^2$ is the Grashof number, and $P=\nu_1/\chi_1$ is the Prandtl number determined by the parameters of the top layer; $\mathbf{e}$ is the unit vector of the axis z.

On the horizontal rigid plates, the boundary conditions read as

$$\mathbf{v}_1 = 0, \quad T_1 = 0 \quad \text{at} \quad z = 1, \quad (4)$$

$$\mathbf{v}_3 = 0, \quad T_3 = 1 \quad \text{at} \quad z = -a - a_*. \quad (5)$$

We assume that the interfaces between fluids are flat and situated at $z=0$ and $z=-a$ and put the following system of boundary conditions at $z=0$:

$$\frac{\partial v_{1x}}{\partial z} - \eta^{-1}\frac{\partial v_{2x}}{\partial z} - \frac{M}{P}\frac{\partial T_1}{\partial x} = 0,$$

$$\frac{\partial v_{1y}}{\partial z} - \eta^{-1}\frac{\partial v_{2y}}{\partial z} - \frac{M}{P}\frac{\partial T_1}{\partial y} = 0, \quad (6)$$

$$v_{1x} = v_{2x}, \quad v_{1y} = v_{2y}, \quad v_{1z} = v_{2z} = 0, \quad (7)$$

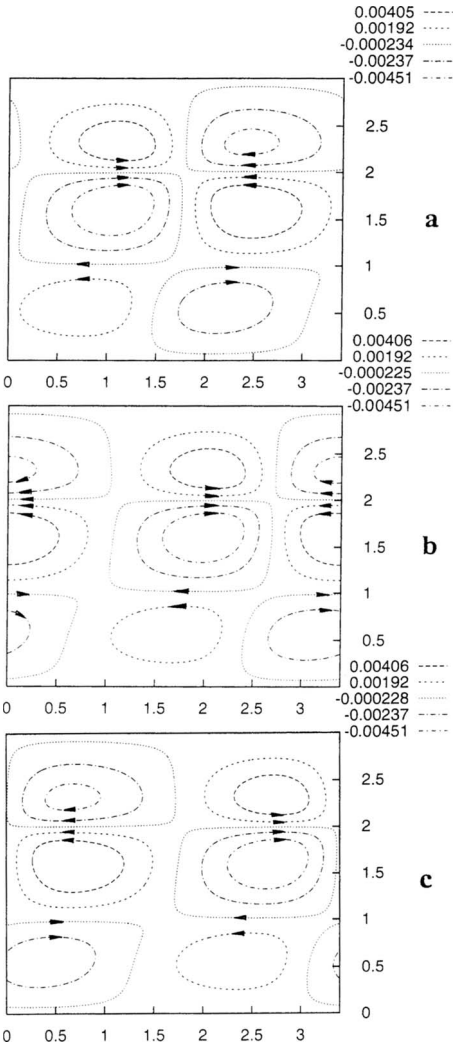

FIG. 2. [(a)–(c)] Snapshots of stream lines for a buoyant-thermocapillary traveling wave at $M=5700$, $G=2.15$, and $L=3.4$.

$$T_1 = T_2, \quad (8)$$

$$\frac{\partial T_1}{\partial z} - \kappa^{-1}\frac{\partial T_2}{\partial z} = 0, \quad (9)$$

at $z=-a$

$$\eta^{-1}\frac{\partial v_{2x}}{\partial z} - \eta_*^{-1}\frac{\partial v_{3x}}{\partial z} - \frac{\bar{\alpha}M}{P}\frac{\partial T_3}{\partial x} = 0, \quad (10)$$

$$\eta^{-1}\frac{\partial v_{2y}}{\partial z} - \eta_*^{-1}\frac{\partial v_{3y}}{\partial z} - \frac{\bar{\alpha}M}{P}\frac{\partial T_3}{\partial y} = 0, \quad (10)$$

$$v_{2x} = v_{3x}, \quad v_{2y} = v_{3y}, \quad v_{2z} = v_{3z} = 0, \quad (11)$$

$$T_2 = T_3, \quad (12)$$

$$\kappa^{-1}\frac{\partial T_2}{\partial z} - \kappa_*^{-1}\frac{\partial T_3}{\partial z} = 0. \quad (13)$$

Here $M=\alpha\theta a_1/\eta_1\chi_1$ is the Marangoni number.

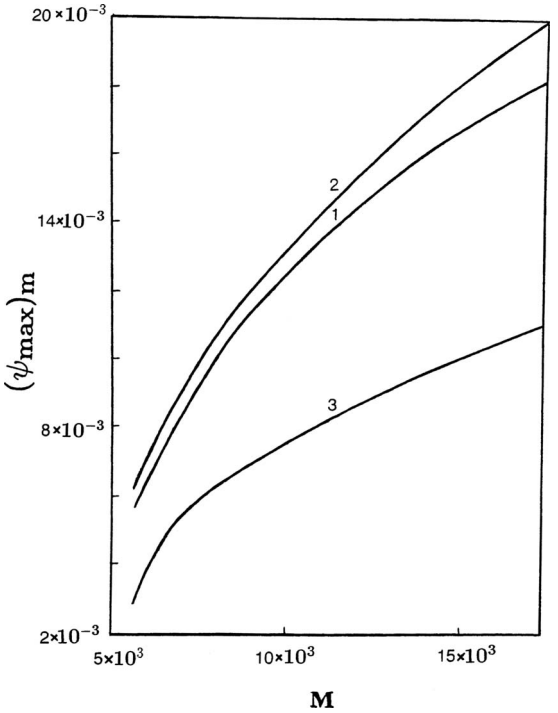

FIG. 3. Dependence of the maximum values of stream function $\psi_{max,m}(m=1,2,3)$ on M for the buoyant-thermocapillary traveling wave at $K=3682$ and $L=3.4$.

The boundary-value problem has a solution

$$\mathbf{v}_m = 0, \quad m = 1,2,3, \tag{14}$$

$$T_1 = T_1^0 = -\frac{(z-1)}{1+\kappa a + \kappa_* a_*}, \tag{15}$$

$$T_2 = T_2^0 = -\frac{(\kappa z - 1)}{1+\kappa a + \kappa_* a_*}, \tag{16}$$

$$T_3 = T_3^0 = -\frac{\kappa_* z - 1 + (\kappa_* - \kappa)a}{1+\kappa a + \kappa_* a_*}, \tag{17}$$

corresponding to the mechanical equilibrium.

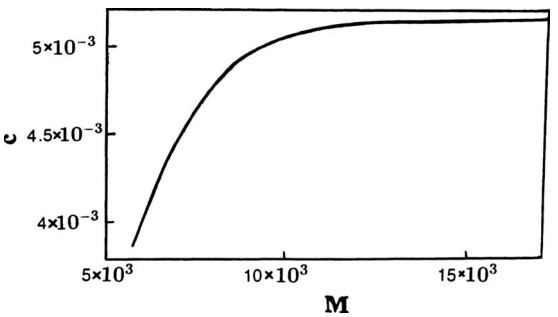

FIG. 4. Dependence of the wave velocity c on the Marangoni number M for the traveling wave; $K=3682$ and $L=3.4$.

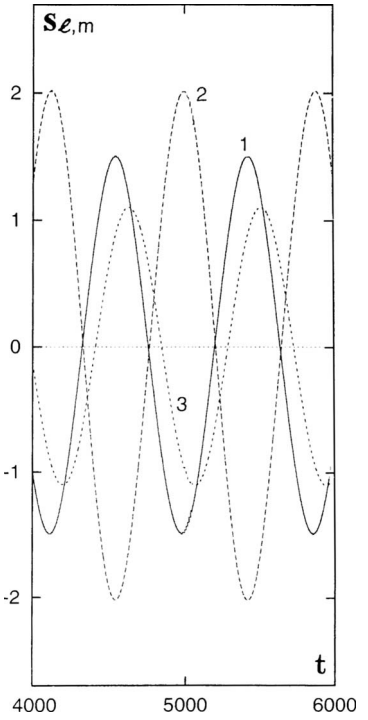

FIG. 5. The dependence of $S_{l,m}$ on time $(m=1,2,3)$ at $M=5700$, $G=2.15$; $L=3.4$.

III. NONLINEAR APPROACH

In order to investigate the flow regimes in a finite region $-l/2 \le x \le l/2$, $-a_2 - a_3 \le z \le a_1$ (see Fig. 1), we perform nonlinear simulations of two-dimensional flows [$v_{my}=0$ $(m=1,2,3)$; the fields of physical variables do not depend on y]. In this case, we can introduce the stream function ψ

$$v_{mx} = \frac{\partial \psi_m}{\partial z}, \quad v_{mz} = -\frac{\partial \psi_m}{\partial x}, \quad (m=1,2,3).$$

Eliminating the pressure and defining the vorticity

$$\phi_m = \frac{\partial v_{mz}}{\partial x} - \frac{\partial v_{mx}}{\partial z},$$

we rewrite the boundary-value problems (1)–(13) in terms of variables ϕ_m, ψ_m, and T_m.

For simulations of cellular motions in an infinite layers, the periodic boundary conditions have been used on lateral walls $x = \pm L/2$, $L = l/a_1$,

$$\psi_m(x+L,z) = \psi_m(x,z); \quad \phi_m(x+L,z) = \phi_m(x,z);$$

$$T_m(x+L,z) = T_m(x,z). \tag{18}$$

The boundary-value problem formulated above was solved by the finite-difference method. Equations were approximated on a uniform mesh using a second-order approximation for the spatial coordinates. The nonlinear equations were solved, using the explicit scheme, on a rectangular uniform mesh 56×112. We checked the results on 56×168 and 112×168 meshes. The relative changes in the stream function amplitudes for all the mesh sizes do not exceed 2.5%. The time step was calculated by the formula

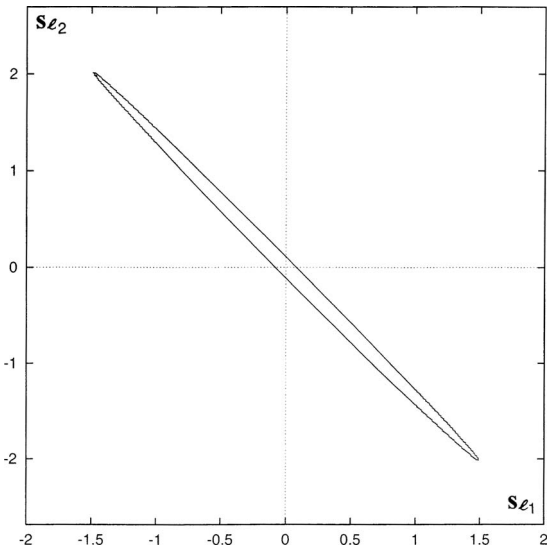

FIG. 6. Phase trajectory $S_{l2}(S_{l1})$ for the oscillatory motion at $M=5700$, $G=2.15$, and $L=3.4$.

$$\Delta t = \frac{[\min(\Delta x, \Delta z)]^2[\min(1, \nu, \chi, \nu_*, \chi_*)]}{2[2 + \max|\psi_m(x,z)|]},$$

where Δx and Δz are the mesh sizes for the corresponding coordinates. The Poisson equations were solved by the iterative Liebman successive over-relaxation method on each time step. The accuracy of the solution was 10^{-4} for the steady motion and 10^{-5} for the oscillations.

The details of the numerical method can be found in the book by Simanovskii and Nepomnyashchy [3] (see also [20]).

IV. NUMERICAL RESULTS

Let us consider the system air-ethylene glycol-fluorinert FC75 with the following set of parameters: $\nu=0.974$, $\nu_*=18.767$, $\eta=0.001$, $\eta_*=0.013$, $\kappa=0.098$, $\kappa_*=0.401$, $\chi=215.098$, $\chi_*=606.414$, $\beta=5.9$, $\beta_*=2.62$, $P=0.72$, and $\bar{\alpha}=0.080$, and fix the ratios of the layers thicknesses $a=a_*=1$.

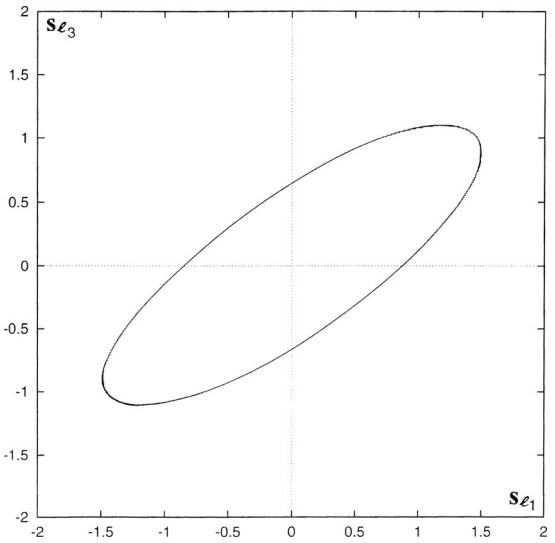

FIG. 7. Phase trajectory $S_{l3}(S_{l1})$ for the oscillatory motion at $M=5700$, $G=2.15$, and $L=3.4$.

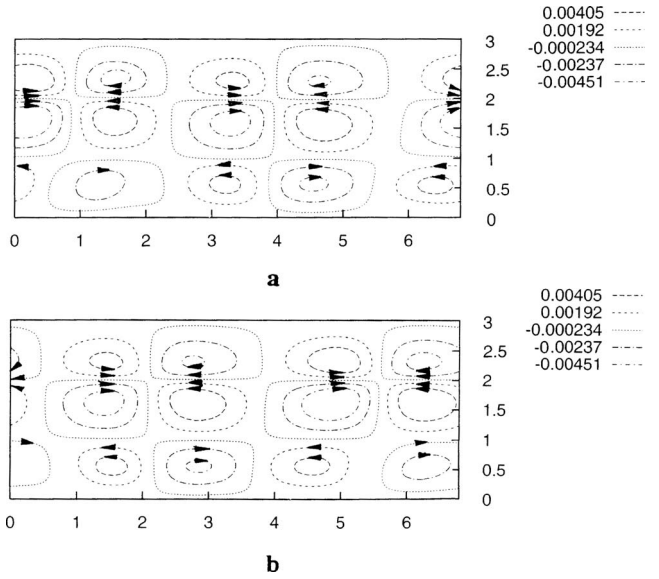

FIG. 8. [(a) and (b)] Snapshots of streamlines for a buoyant-thermocapillary traveling wave at $M=5700$, $G=2.15$, and $L=6.8$.

This system has been chosen because of the following reasons. First of all, this system is appropriate for Earth experiments because of the relatively low viscosity of the fluorinert (see [23]). Scientific interest in this system is owing to the fact that it is subject to different kinds of instabilities driven by different interfaces. For the system under consideration, the flow of the thermocapillary origin takes place mainly near the upper interface. The flow of the buoyancy origin is developed mainly in the bottom layer. The indirect interaction of both mechanisms of instability can lead to a much more complex dynamics (in comparison with two-layer systems) and various unexpected effects. Evidently,

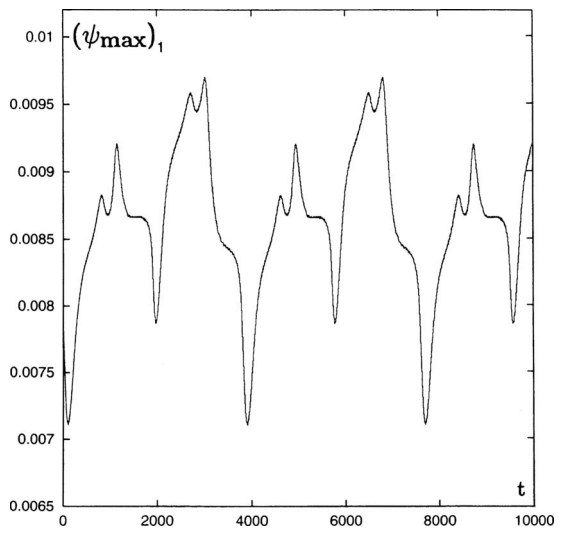

FIG. 9. The dependence of the maximum values of stream function $\psi_{max,1}$ on t for the pulsating traveling wave at $M=7000$, $G=5$, and $L=3.4$.

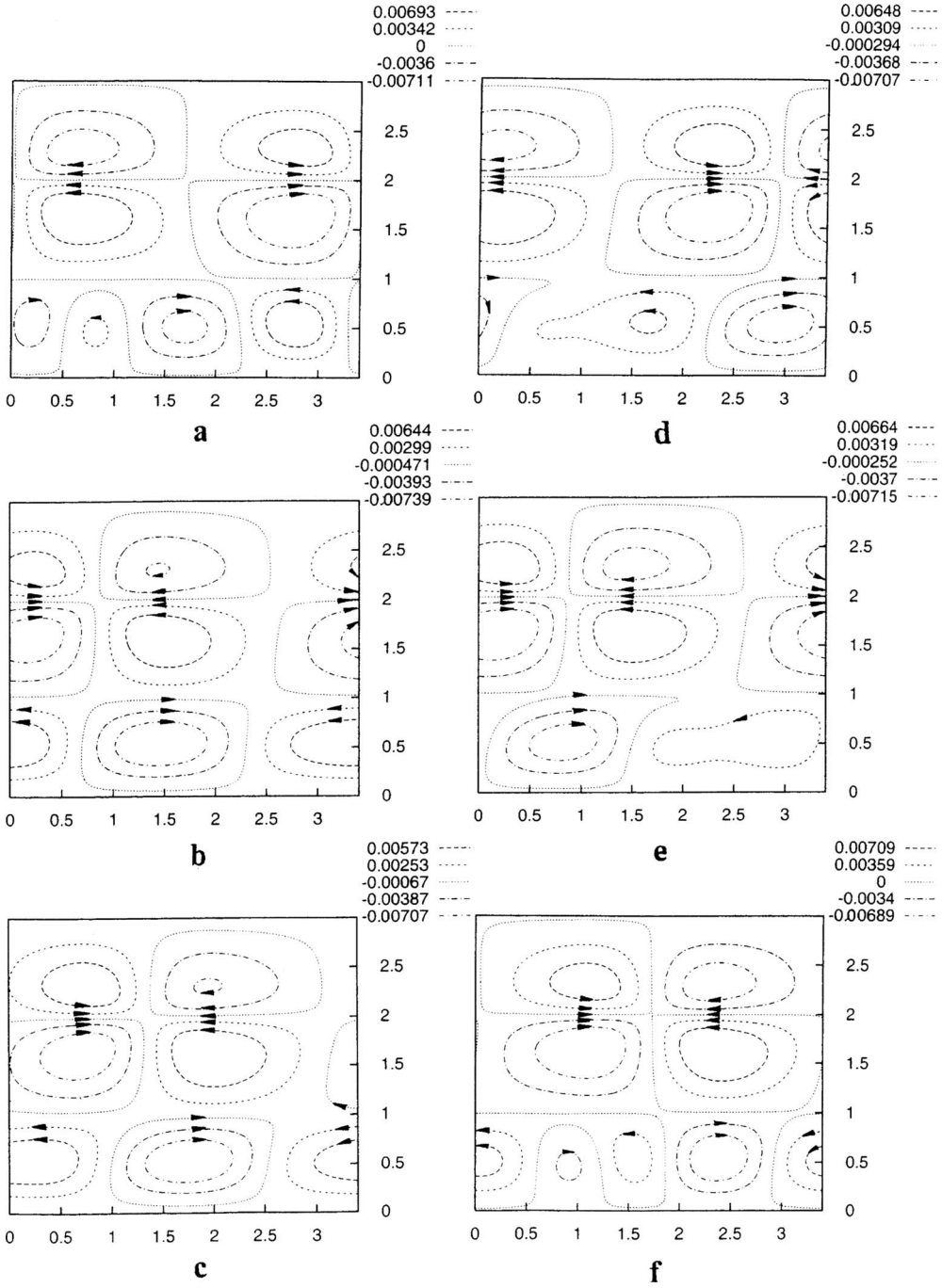

FIG. 10. [(a)–(f)] Snapshots of streamlines for the pulsating traveling wave at $M=7000$, $G=5$, and $L=3.4$.

such an indirect interaction is impossible in the system with a single interface.

Let us describe the results of nonlinear simulations. Two types of stationary flows have been found: (1) the Marangoni flow slightly influenced by buoyancy and (2) buoyancy flow slightly influenced by the thermocapillary effect. The flow of the thermocapillary origin takes place around the upper interface (i.e., mainly in the top and middle layers) and the flow of the buoyancy origin is developed mainly in the bottom layer.

Now, let us consider the joint action of both instability mechanisms. Above the threshold predicted by the linear stability theory (see [27]), the specific type of *nonlinear traveling wave* is developed

$$\psi_m(x,z,t) = \psi_m(x-ct,z), \quad T_m(x,z,t) = T_m(x-ct,z), \qquad (19)$$

where c is the phase velocity of the traveling wave.

Snapshots of streamlines for the buoyant-thermocapillary traveling wave at different moments of time are presented in Fig. 2. The traveling wave moves from the right to the left. Certainly, the wave moving in the opposite direction is also possible. The maximum values of stream functions in all the layers $\psi_{max,m}=\max \psi_m(x,z)(m=1,2,3)$ are constant in time.

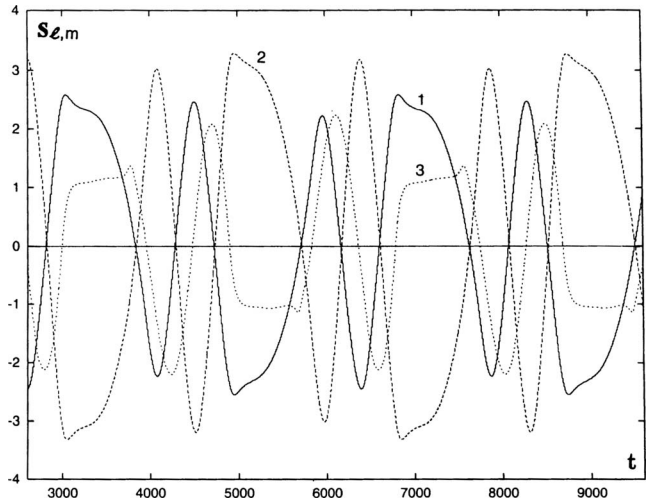

FIG. 11. The dependence of $S_{l,m}$ on time $(m=1,2,3)$ at $M=7000$, $G=5$, and $L=3.4$.

Under the conditions of the experiment, when the geometric configuration of the system is fixed while the temperature difference θ is changed, the Marangoni number M and the Grashof number G are proportional. We define the inverse dynamic Bond number

$$K = \frac{M}{GP} = \frac{\alpha}{g\beta_1\rho_1 a_1^2}.$$

The dependencies of $\psi_{max,m}$ $(m=1,2,3)$ on M for the fixed value of K are shown in Fig. 3. One can see that the most intensive motion takes place in the middle layer. With the increase in the Marangoni number, the period of the wave decreases, i.e., the phase velocity grows. The dependence of the phase velocity $c(M)$ is presented in Fig. 4.

We use the following integral quantities, characterizing the intensity of motions in the left and in the right halves of the layers:

$$S_{l1}(t) = \int_{-L/2}^{0} dx \int_{0}^{1} dz \psi_1(x,z,t),$$

$$S_{r1}(t) = \int_{0}^{L/2} dx \int_{0}^{1} dz \psi_1(x,z,t), \tag{20}$$

$$S_{l2}(t) = \int_{-L/2}^{0} dx \int_{-a}^{0} dz \psi_2(x,z,t),$$

$$S_{r2}(t) = \int_{0}^{L/2} dx \int_{-a}^{0} dz \psi_2(x,z,t), \tag{21}$$

$$S_{l3}(t) = \int_{-L/2}^{0} dx \int_{-a-a_*}^{-a} dz \psi_3(x,z,t),$$

$$S_{r3}(t) = \int_{0}^{L/2} dx \int_{-a-a_*}^{-a} dz \psi_3(x,z,t). \tag{22}$$

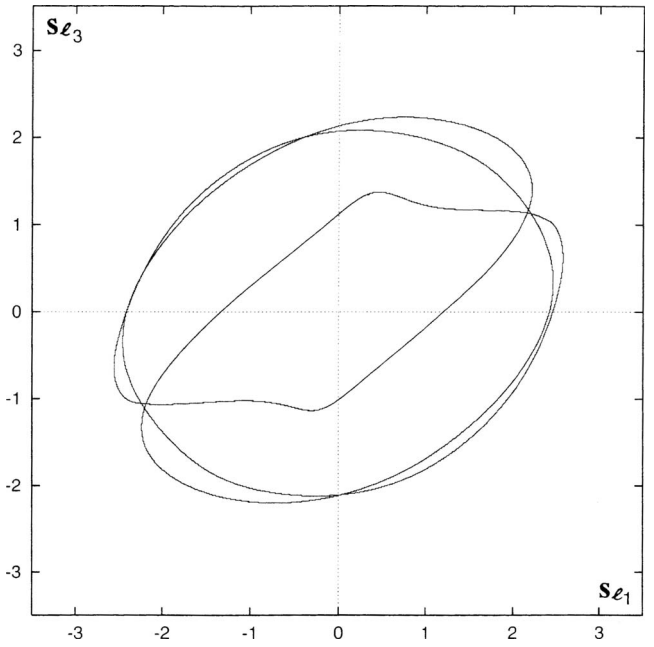

FIG. 12. Phase trajectory $S_{l3}(S_{l1})$ for the pulsating traveling wave at $M=7000$, $G=5$, and $L=3.4$.

The time evolution of the quantities $S_{lm}(t)$, $m=1,2,3$, is shown in Fig. 5. One can see that oscillations keep rather simple almost sinusoidal form. The phase trajectory in Fig. 6 demonstrates that the oscillations in the top layer and in the middle layer take place almost out of phase. The phase trajectory presented in Fig. 7 shows a significant phase delay of the oscillations in the top layer with respect to the oscillations in the bottom layer. Let us emphasize that even on a large distance from the linear stability boundary (see line 3 in Fig. 5 of [27]; $M \leq 228\,000$), the oscillatory flow keeps its periodicity for the fixed value of K $(K=3682)$. For this motion, the thermocapillary convection in the top and middle layers coexists with the buoyancy convection in the bottom layer. (Let us note that in the case of the cavity with rigid heat-insulated lateral boundaries [27], the region of the oscillatory flow in the $(G,\ M)$ plane had very small finite area and was surrounded by the regions of the mechanical equilibrium and steady flows). In a long computational region with $L=6.8$, the traveling wave described above keeps its perfect periodicity (see Fig. 8). Thus, there is no long-wave modulational instability for buoyant-thermocapillary traveling wave at the moderate values of M and G.

Let us discuss now the evolution of flow regimes by changing the inverse dynamic Bond number: we fix $K=1944$. The decrease of K (the weakening of the thermocapillary effect) leads to the appearance of a new convective regime: the buoyant-thermocapillary wave is destabilized and the *pulsating traveling wave* is developed in the system. The maximum values of stream function $(\psi_{max,m})$ $(m=1,2,3)$ are not constant in time any more and oscillate in a periodic way. As an example, we present the dependence of $(\psi_{max,1})(t)$ in the top layer (see Fig. 9).

Snapshots of stream lines at different moments of time corresponding to the pulsating traveling wave are presented in Fig. 10. The vortices change their form and intensity dur-

ing the oscillatory process. One can see the merging and the recombination of vortices with different sizes in the bottom layer.

The time evolution of quantities $S_{lm}(t)$, $m=1,2,3$, is shown in Fig. 11. The oscillations become rather complicated, keeping the periodic form. The most intensive motion takes place in the middle layer. The multiloop phase trajectory, corresponding to the pulsating traveling wave, is presented in Fig. 12.

V. CONCLUSION

The nonlinear regimes of convection in a multilayer system where the Marangoni convection is produced by the upper interface and hence developed in the top layer and in the middle layer, while the buoyancy convection is produced in the bottom layer, are investigated. The periodic boundary conditions on the lateral boundaries are considered. It is shown that the joint action of buoyancy and thermocapillary effect leads to the development of a specific type of nonlinear traveling wave. For this motion, the thermocapillary convection in the top and middle layers coexists with the buoyancy convection in the bottom layer. The oscillatory flow keeps its periodicity even on a large distance from the linear stability boundary. The weakening of the thermocapillary effect leads to the development of the pulsating traveling wave in the system. The maximum values of the stream function in all the layers oscillate in a periodic way. The vortices change their form and intensity during the oscillatory process.

[1] G. Z. Gershuni and E. M. Zhukhovitsky, *Convective Stability of Incompressible Fluid* (Keter, Jerusalem, 1976).
[2] J. R. A. Pearson, J. Fluid Mech. **4**, 489 (1958).
[3] I. B. Simanovskii and A. A. Nepomnyashchy, *Convective Instabilities in Systems with Interface* (Gordon and Breach, London, 1993).
[4] D. Johnson and R. Narayanan, Chaos **9**, 124 (1999).
[5] A. Nepomnyashchy, I. Simanovskii, and J.-C. Legros, *Interfacial Convection in Multilayer Systems* (Springer, New York, 2006).
[6] D. A. Nield, J. Fluid Mech. **19**, 341 (1964).
[7] A. Juel, J. M. Burgess, W. D. McCormick, J. B. Swift, and H. L. Swinney, Physica D **143**, 169 (2000).
[8] J. Burguete, N. Mukolobwiez, N. Daviaud, N. Garnier, and A. Chiffaudel, Phys. Fluids **13**, 2773 (2001).
[9] J. Priede and G. Gerbeth, Phys. Rev. E **56**, 4187 (1997).
[10] S. Madruga, C. Perez-Garcia, and G. Lebon, Phys. Rev. E **68**, 041607 (2003).
[11] A. Nepomnyashchy and I. Simanovskii, Phys. Fluids **18**, 032105 (2006).
[12] M. Wanschura, H. C. Kuhlmann, and H. J. Rath, Phys. Rev. E **55**, 7036 (1997).
[13] D. E. Melnikov, V. M. Shevtsova, and J. C. Legros, Phys. Fluids **16**, 1746 (2004).
[14] D. E. Melnikov, Ph.D. thesis, Université Libre de Bruxelles, 2004.
[15] M. Kassemi and N. Rashidnia, Phys. Fluids **12**, 3133 (2000).
[16] T. Doi and J. N. Koster, Phys. Fluids A **5**, 1914 (1993).
[17] P. Georis and J.-C. Legros, in *Materials and Fluids under Low Gravity*, edited by L. Ratke, H. Walter, and B. Feuerbacher (Springer-Verlag, Berlin, 1996), pp. 299–311.
[18] H. Groothuis and F. G. Zuiderweg, Chem. Eng. Sci. **12**, 288 (1960).
[19] I. B. Simanovskii, Physica D **102**, 313 (1997).
[20] A. A. Nepomnyashchy and I. B. Simanovskii, Phys. Rev. E **59**, 6672 (1999).
[21] I. B. Simanovskii, Eur. J. Mech. B/Fluids **19**, 123 (2000).
[22] A. Prakash, D. Fujita, and J. N. Koster, Eur. J. Mech. B/Fluids **12**, 15 (1993).
[23] A. Prakash and J. N. Koster, Eur. J. Mech. B/Fluids **12**, 635 (1993).
[24] I. B. Simanovskii, Eur. J. Mech. B/Fluids **26**, 422 (2007).
[25] I. B. Simanovskii, Phys. Fluids **19**, 082106 (2007).
[26] A. A. Nepomnyashchy and I. B. Simanovskii, Fluid Dyn. **19**, 494 (1984).
[27] A. A. Nepomnyashchy, I. B. Simanovskii, and L. M. Braverman, Phys. Fluids **17**, 022103 (2005).